LARGE-EDDY SIMULATION OF HUMAN PHONATION USING THE ANISOTROPIC MINIMUM-DISSIPATION MODEL

M. Lasota[1,3], P. Šidlof[1,2]

[1] Faculty of Mechatronics, Technical University of Liberec, Studentská 2, 461 17 Liberec 1, Czech Republic
[2] Institute of Thermomechanics, Czech Academy of Sciences, Dolejškova 5, 182 00 Prague 8, Czech Republic
[3] Department of Technical Mathematics, CTU in Prague, Karlovo náměstí 13, 121 35 Prague 2, Czech Republic

Abstract: ***This contribution is focused on numerical modeling of 3D incompressible laryngeal flow through healthy vocal folds oscillating at a fundamental frequency of 100 Hz. The investigation is based on a realistic CFD simulation of turbulent flow by Large-Eddy Simulation with various subgrid-scale models and monitoring their influence on the aeroacoustic spectrum during human phonation of five vowels /u, i, a, o, æ/.***

Keywords: **human phonation, turbulent flow, aeroacoustic simulations, vocal tract shapes, vowels**

I. INTRODUCTION

Voice production has been investigated by experimental measurements and numerical simulations. However, the experiments often bring numerous limitations, especially when the in-vivo measurements have to be carried out. High-performance computing can be used as an alternative method An extensive list of numerical models of human phonation is available in [1]. The current contribution presents a computational aeroacoustic model of human phonation based on high-resolution Large-Eddy Simulation (LES) of glottal flow with advanced turbulence modeling.

II. METHODS

Considering the enormous disparity of scales in the flow and acoustics, the aeroacoustic simulation has been divided by computing the flow by the finite-volume method, and subsequently the sound sources and wave propagation by the finite-element method, for more details, see [2]. The Large-Eddy Simulation of flow resolves the large-scale vortices, while the influence of the subgrid-scale vortices is modeled by a subgrid-scale closure model. Various subgrid-scale models have been studied to cope with near-wall modeling in the glottis, where inaccurate prediction of the shear stress at the surface of vocal folds delays the transition to turbulence. The dominant sound source caused by flow-induced vibration of vocal folds lie within the glottis. Thereby the geometry and kinematics were specified with care, but some necessary simplification had to be included.

Fig. 1 presents the simplified 3D model of the larynx in a coronal view with a square cross-section in the straight subglottal and supraglottal segments 12x12 mm (y-z plane). The kinematics of vocal folds is prescribed by sinusoidal displacement of inferior-superior margins in medial-lateral (y) direction with two degrees of freedom with the amplitude A=0.3 mm for both vocal folds, allowing closing/opening the glottal gap g in the range 0.42-1.46 mm, having the medial surface convergence angle $\psi/2$ (in clockwise) for convergent and divergent position -10° and +10°, respectively, and with the same phase difference $\pi/2$ between the inferior and superior vocal fold margin on both vocal folds. The distance (y) between both ventricles and false vocal folds is equal to 16 and 6.15 mm, respectively. The boundary conditions for the fluid flow are listed in Tab. 1.

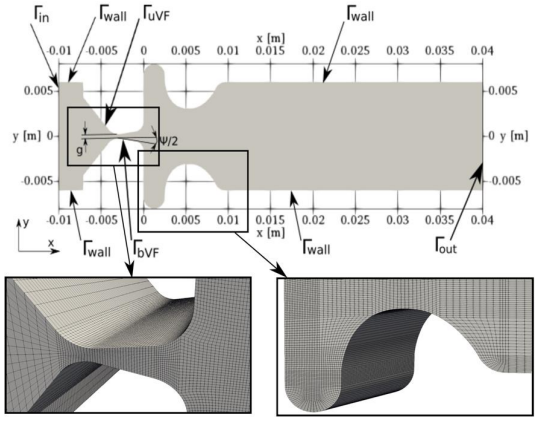

Figure 1 - Geometry, boundaries and mesh of the larynx

Table 1 – Boundary conditions of filtered flow variables velocity and static pressure.

Boundary	$\overline{\boldsymbol{U}}$ [ms^{-1}]	$\overline{p}$ [Pa]
Inlet Γ_{in}	from flux, $\overline{U}_i n_i < 0$ $0, \overline{U}_i n_i > 0$	307.4
Outlet Γ_{out}	$\nabla(\overline{\boldsymbol{U}}) \cdot \boldsymbol{n} = 0, \overline{U}_i n_i > 0$ $\overline{\boldsymbol{U}} = 0, \overline{U}_i n_i < 0$	0
Vocal folds Γ_{bVF}, Γ_{uVF}	$\overline{U}_2 = \frac{\partial}{\partial t} h(\boldsymbol{x}, t)$ $\overline{U}_1 = \overline{U}_3 = 0$	$\nabla(\overline{p}) \cdot \boldsymbol{n} = 0$
Fixed walls Γ_{wall}	$\overline{\boldsymbol{U}} = 0$	$\nabla(\overline{p}) \cdot \boldsymbol{n} = 0$

Healthy phonation reaches the Reynolds number in the range (100-10,000), thereby the flow field is highly turbulent. The large eddies carrying the most energy in the flow are resolved directly by Navier-Stokes equations (NSE), whereas the small scales are modeled applying a spatial filter ($\bar{\cdot}$) to the NSE, that gives

$$\partial_t + \partial_j(\bar{u}_i\bar{u}_j) - \partial_j(\nu\partial_j\bar{u}_i) = -\partial_i(\bar{p}) - \partial_j\tau_{ij},\ \partial_i\bar{u}_i = 0, \quad (1)$$

where the subgrid-scale tensor $\tau_{ij}(u)$ represents the effect of small scales on directly resolved large eddies. To include local increasing of turbulent (eddy) viscosity ν_t from the unresolved eddies into molecular viscosity ν is applied the eddy-viscosity equation

$$\tau_{ij} - \frac{1}{3}\tau_{kk}I_{ij} = -2\nu_t S_{ij}, \quad (2)$$

where I_{ij} is the identity matrix and S_{ij} is resolved rate-of-strain tensor. This study is focused on approximation of ν_t by various turbulence subgrid-scale models, namely the standard One-Equation (OE) [3], Wall-Adapting Local-Eddy (WALE) [4] and a newly implemented Anisotropic Minimum Dissipation (AMD) model [5]. For completeness, the fourth case (LAM) is included with no turbulence modeling. The used acoustic grids are shown in Figs. 2-6, varying in shapes for each vowel.

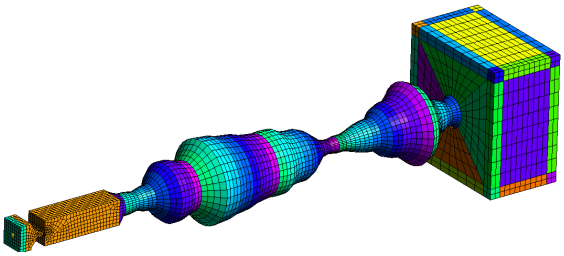

Figure 2 - Acoustic mesh for /u/

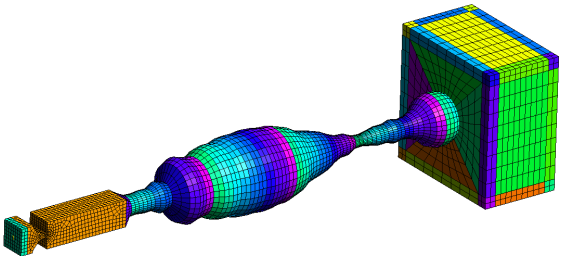

Figure 3 - Acoustic mesh for /i/

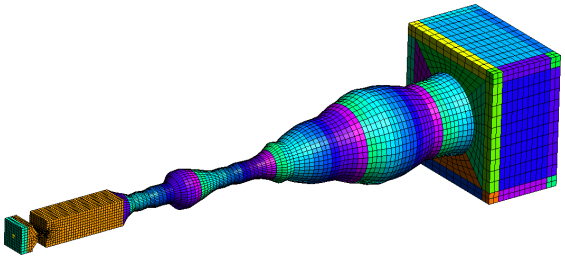

Figure 4 - Acoustic mesh for /a/

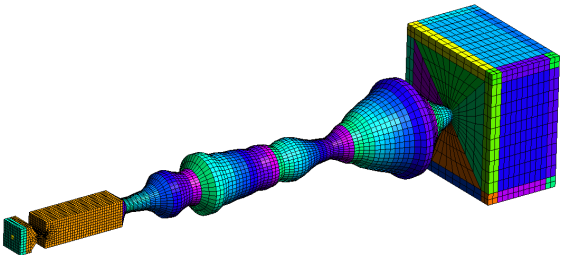

Figure 5 - Acoustic mesh for /o/

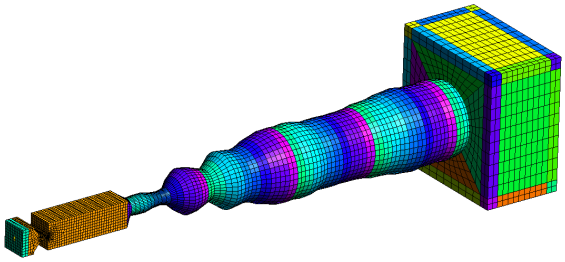

Figure 6 - Acoustic mesh for /œ/

At the laryngeal and vocal tract walls, a sound-hard boundary condition perfectly reflecting the sound waves are specified. At the boundary of the radiation region and subglottal inlet, a Perfectly Matched Layers suppressing the acoustic reflections are used. The Perturbed Convective Wave Equations [6] were used to solve the acoustic potential ψ^a from the partial differential equation

$$\frac{1}{c_0^2}\frac{D^2\psi^a}{Dt^2} - \nabla\cdot\nabla(\psi^a) = -\frac{1}{\rho c_0^2}\frac{D\bar{p}^{ic}}{Dt}, \quad (3)$$

where the acoustic potential is equal to the acoustic pressure in this case of $\rho \approx 1$. The probe location MIC1 (Fig. 7), 1 cm from mouth, is used for the Fast Fourier Transform ($\Delta f \approx 5$ Hz).

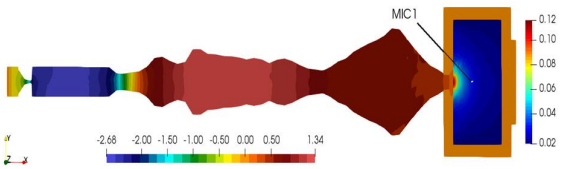

Figure 7 – Coronal view of the computational domain for /o/. Distribution of acoustic potential $\psi^a(t)$

III. RESULTS

Four CFD simulations over 20 periods of vocal fold oscillations were realized, with subsequent aeroacoustic simulations yielding the acoustic spectra (Figs. 8-12). The usage of subgrid-scale turbulence models does not modify positions of formant frequencies, but it modifies considerably the SPLs. The simulations using the new AMD model enforced higher harmonics compared the rest of models, except the higher harmonics in the spectrum of vowel /i/.

Vowel /u/. SPLs at F_2=1000 Hz and $F_3 \approx$ 2500 Hz are nonuniform, at the second formant AMD is higher by 22 % than WALE, and subsequently at the third formant WALE is higher by 28 % than AMD. This trend occurs only for vowels /u, *a*/.

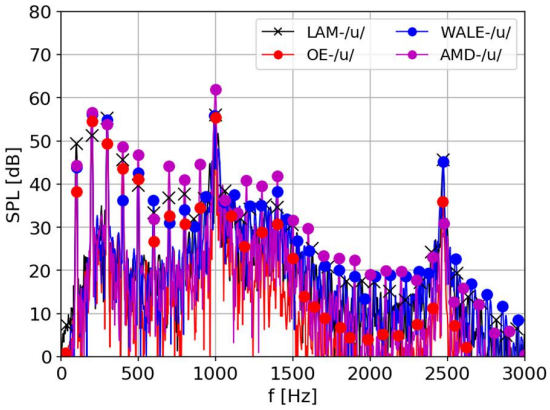

Figure 8 - Acoustic sound spectrum for /u/

Vowel /i/. At f_o=100 Hz the SPL for the AMD model refers to a very low value around 35 dB, whereas the other SPLs are minimally 17 % higher. In general the SPLs for the AMD model are low in low-frequency bandwidth, but for the $F_2 \approx$1400 Hz the AMD model is enforced by 21 % compared to WALE. In the situation at F_3=2500 Hz the WALE and AMD models are close to each other and 1-2 dB higher than the laminar case. This could mean that the AMD and WALE model have a similar behavior at high-frequency bandwidth, but this assumption holds only for /i, o, æ/. The WALE model also enforced the sound pressure levels at F_2 and F_3 stronger than the OE model, by 6-8 dB and 7-15 dB, respectively, which is related to higher flow rate through the glottis.

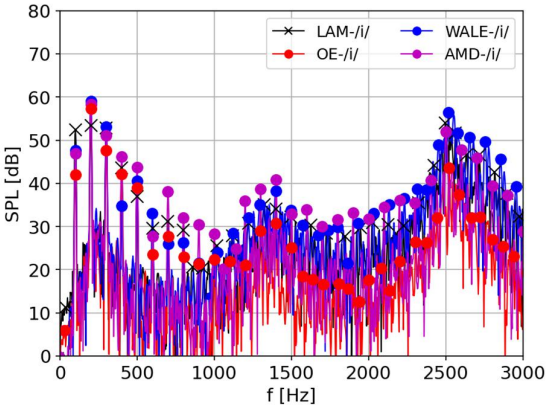

Figure 9 - Acoustic sound spectrum for /i/

Vowel /a/. SPLs at f_o stayed at similar levels for the WALE and AMD models, which happened only twice, in cases /*a*, æ/. The space between formants F_1-F_2 is typical for vowels /u, *a*, o/, but in simulation of /*a*/ the second formant (around 1300 Hz) was not distinct. On the other hand, the third formant is clearly visible and presents the same behavior as it was seen in /u/, i.e. a big drop predicted by AMD up to 9 and 13 dB compared to WALE and LAM, respectively.

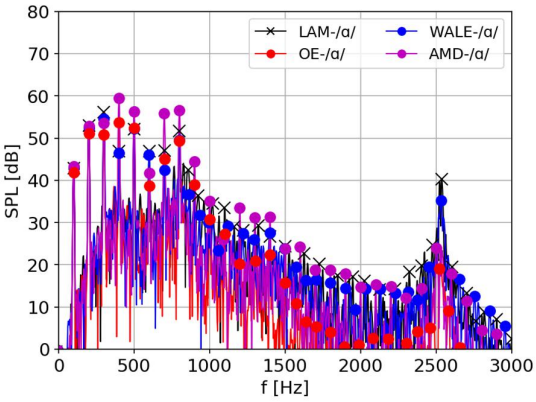

Figure 10 - Acoustic sound spectrum for /a/

Vowel /o/. The SPLs are held at high levels up to 3 kHz, with some little skips, however the vocal tract shape (see again Fig. 5 and 7) has contained the widest throat 7.25 cm^2 of presented acoustic grids.

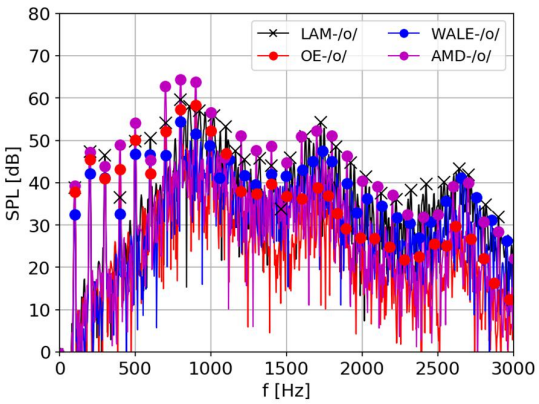

Figure 11 - Acoustic sound spectrum for /o/

Vowel /æ/. In this case, the AMD model highlighted the first formant very well, 14 dB higher than the WALE. The predictions of the SPL of the second and third formants by various SGS models were similar, with differences less than 3 dB.

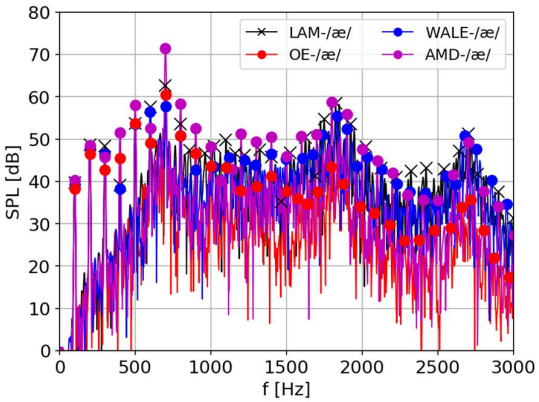

Figure 12 - Acoustic sound spectrum for /æ/

IV. Discussion

So far, the AMD subgrid-scale model has not been studied in the application associated with human phonation. In addition, the computational efforts can be reduced compared to conventional subgrid-scale models, due to the more accessible algorithm computing no invariants from the rate-of-strain tensor.

V. Conclusion

In the result section was demonstrated that the subgrid-scale models have a considerable impact on sound pressure levels. In the simulations using the OE model, formants were hardly visible and significantly weaker compared to other models. Usage of the WALE model, which is well-known to handle the turbulent viscosity at near-wall and high-shear regions more precisely than the OE model, predicted 7% higher volumetric flow rates of air through the glottis compared to the OE model, and only slightly lower than the LAM and AMD models (by 9 and 4 %, respectively). The (widely-used) WALE model was able to uncover all characteristics for identification of formant frequencies, even so it gave the best recognition of third formants in high-frequency bandwidth in cases /u, *a*/. In contrary, the newly implemented AMD model has proven a good agreement with the WALE model, and even more it identified the SPLs at lower formants F_1 and F_2 the most evident, with the exception of the vowel /i/.

The research was supported by the Czech Science Foundation, project 19-04477S Modelling and measurements of fluid-structure-acoustic interactions in biomechanics of human voice production, and by the Student Grant Scheme at the Technical University of Liberec through project no. SGS-2020-3068.

REFERENCES

[1] Alipour, F., Brücker, C., Cook, D., Gömmel, A., Kaltenbacher, M., Willy, M., et al. Mathematical models and numerical schemes for the simulation of human phonation. *Current Bioinformatics.* **2011**, 6(3).

[2] Lasota, M.; Šidlof, P.; Kaltenbacher, M.; Schoder, S. Impact of the Sub-Grid Scale Turbulence Model in Aeroacoustic Simulation of Human Voice. *Appl. Sci.* **2021**, *11*, 1970. https://doi.org/10.3390/app11041970

[3] Davidson, L. Hybrid LES-RANS: back scatter from a scale-similarity model used as forcing. *Philosophical Transactions of the Royal Society A: Mathematical, Physical and Engineering Sciences*. **2009**. Vol. 367. No. 1899. pp. 2905-2915.

[4] Nicoud, F. and Ducros, F. Subgrid-scale stress modelling based on the square of the velocity gradient tensor. *Flow, Turbulence and Combustion*. **1999**. Vol. 62. No. 3. pp. 183-200.

[5] Rozema, W., Bae, H., Moin, P. and Verstappen, R. Minimum-dissipation models for large-eddy simulation. *Physics of Fluids*. **2015**. Vol 27. No. 8.

[6] Hüppe, A., Grabinger, J., Kaltenbacher, M., Reppenhagen, A., Dutzler, G., Kühnel, W. A non-conforming finite element method for computational aeroacoustics in rotating systems. *20th AIAA/CEAS Aeroacoustics Conference.* 2014.